Available online at www.sciencedirect.com

ScienceDirect

Proceedings of the Combustion Institute 39 (2023) 1415–1423

Proceedings of the Combustion Institute

www.elsevier.com/locate/proci

Chemiluminescent footprint of premixed ammonia-methane-air swirling flames

Syed Mashruk [a,*], Xuren Zhu [b,*], William L. Roberts [b], Thibault F. Guiberti [b], Agustin Valera-Medina [a]

[a] College of Physical Sciences and Engineering, Cardiff University, Wales, CF24 3AA. UK
[b] CCRC, King Abdullah University of Science and Technology (KAUST), Thuwal 23955-6900, Saudi Arabia

Received 5 January 2022; accepted 23 August 2022
Available online 19 October 2022

Abstract

This work reports on the chemiluminescence signature of premixed ammonia-methane-air swirling flames. Wide ranges of equivalence ratios ($0.6 \leq \Phi \leq 1.3$), ammonia fractions in the fuel blend ($0 \leq X_{NH3} \leq 0.70$), and Reynolds numbers ($10{,}000 \leq Re \leq 40{,}000$) were investigated to understand effects of these parameters on the light emitted by these flames. Excited radicals contributing to chemiluminescence in the UV and visible ranges were confirmed, namely NO*, OH*, NH*, CN*, CO_2*, CH*, and NH_2*. With non-intrusive flame monitoring in mind, various ratios of chemiluminescence intensities were carefully studied because these allow removing effects of time-varying flame surface area that is inherent in turbulent flames. Consistent with previous findings in laminar flames, ratios CN*/OH*, CN*/NO*, and NH*/CH* were found to be promising candidates. Ratios CN*/OH* and CN*/NO* were identified as potential surrogates for equivalence ratio if $X_{NH3} \geq 0.20$ and $0.05 \leq X_{NH3} \leq 0.50$, respectively. Ratio NH*/CH* was identified as a potential surrogate for the ammonia fraction in the fuel blend provided that equivalence ratio is roughly known. Ratio *Blue*/NH_2*, obtained exclusively from measurements in the visible range, is another interesting surrogate for the ammonia fraction but its sensitivity to Reynolds number may limits its range of applications. Trends of measured exhaust NO concentration with equivalence ratio and ammonia fraction were found to qualitatively match that of NO*, NH*, and CN*, implying that emissions from these excited radicals could be used to monitor the NO performance of practical ammonia-methane-air flames.

Keywords: Flame sensor; Flame monitoring; Spontaneous emission; Excited radicals; Turbulence

1. Introduction

The desire to advance combustion diagnostics derives from the need to improve the stability, operability, fuel flexibility, and thermal and emission performances of combustion devices [1]. For example, the precise determination of equivalence ratio has helped to significantly reduce the level of

* Corresponding authors.
E-mail addresses: mashruks@cardiff.ac.uk (S. Mashruk), xuren.zhu@kaust.edu.sa (X. Zhu).

https://doi.org/10.1016/j.proci.2022.08.073

NOx emission in dry-lean gas turbine engines [2]. Combustion diagnostics have also been used for the active control of combustion instabilities based on the on-site monitoring of heat release rate fluctuations, which mainly result from flame surface and equivalence ratio variations [3]. Therefore, numerous efforts have been devoted to develop effective and cost-competitive flame sensing methods [4,5].

Chemiluminescence-based diagnostics have been widely applied to practical flames owing to their non-intrusive, simple, and cheap nature. Chemiluminescence involves the emission of light from excited radicals, such as OH^*, CH^*, and NO^* for example, after they were produced via chemical reactions [6]. Chemiluminescence in hydrocarbon flames has been shown to provide useful information on the location of the reaction zone [7], equivalence ratio [8], and heat release rate [9], hence, it is used to infer indirectly the combustion performance, NOx emission formation, or the integrity of hardware.

Recently, numerous studies have been performed to understand the combustion characteristics of ammonia since ammonia has been recognized as a promising future fuel for carbon free combustion [10,11], with the emphasize on flame stability and NOx emission. Although a number of studies previously reported on some features of the chemiluminescence of ammonia flames (e.g., in [12–15]), it is still unclear how chemiluminescence correlates with relevant flame properties for more practical operating conditions featuring ammonia.

Recently, Zhu et al. [16] employed a counterflow burner to investigate the chemiluminescence signature of laminar premixed ammonia-methane-air flame. Ratios CN^*/OH^* and NH^*/CH^* were found to correlate well with equivalence ratio and ammonia fuel fraction, respectively. This laid the first stone towards the development of optical sensors for flames featuring ammonia in the fuel blend. However, their work was restricted to laminar flames and effects of turbulence were not investigated. Turbulence potentially influences flames through local extinction [17], stretch [18], curvature [19,20], and vortex/flame interactions [21,22] and could, in turn, influence chemiluminescence as well. Given the important role that ammonia will play in tomorrow's energy landscape, it is of interest to understand the chemiluminescence of practical turbulent ammonia flames, eventually leading to the development of chemiluminescence-based sensors for the monitoring of industrial combustion devices. Therefore, the present study focuses on the chemiluminescence of premixed ammonia-methane-air swirl flames, operating for wide ranges of ammonia fuel fraction, equivalence ratio, and Reynolds number.

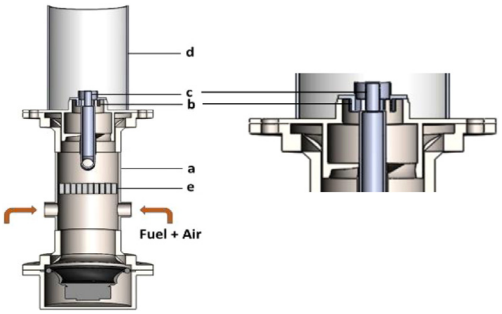

Fig. 1. Cross-sectional view of the burner.

2. Experimental facility and diagnostics

2.1. Optically-accessible swirl combustor

An industrial scale tangential swirl burner with optical access (GE214 quartz material, spectral curve provided in Supplementary Material, Fig. S1) and a geometric swirl number of $S_g = 1.05$, shown in Fig. 1, was operated with different volume fractions of ammonia in the ammonia-methane fuel blends $0 \leq X_{NH3} \leq 1$, equivalence ratios $0.6 \leq \Phi \leq 1.3$, and bulk Reynolds numbers $10{,}000 \leq Re \leq 40{,}000$. Changes in Re were achieved by varying the volumetric flow rates of the combustible mixtures. Gas flow rate were prescribed with Bronkhorst thermal mass flow controllers (accuracy better than ±0.5% within 15–95% of the full scale). From the premix chamber (label a), fuels and air leave the burner's exit nozzle ($r = 28$ mm) through a single radial-tangential swirler (label b), using the central injection lance (label c) as a bluff-body ($r = 16$ mm). The flame was housed within a cylindrical quartz confinement (label d) with an expansion ratio of 3 relative to the burner's exit nozzle. A honeycomb (label e) was installed to homogenize the flow and mitigate risks associated with flashback. Further details of the burner geometry are provided in Supplementary Material, Fig. S2. Experiments were conducted near atmospheric pressure (1.1 bar(a)) and at room temperature (~288 K).

2.2. Chemiluminescence measurements

A UV/visible-capable optical fiber head (Stellernet Inc DLENS with F600 fiber optic cable) was installed 3 cm above the burner's exit and 10 cm away from its central axis, providing a field of view (FOV) of approximately 30 mm × 30 mm at the flame core. The other end of the optical fiber was connected to a UV/visible-capable spectrometer (Stellernet Inc BLUE-Wave) featuring a 100-mm focal length and a 25-μm wide entry slit. The spectrometer was equipped with a 600-grooves/mm

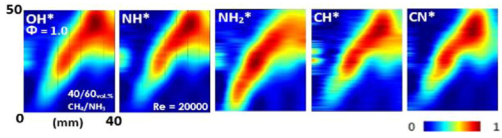

Fig. 2. Inverse Abel transformed images of swirl flame with $X_{NH3} = 0.6$, Re = 20000 and $\Phi = 1.0$ corresponding to the emission from different excited radicals. Colormaps are normalized by the maximum value found in each image.

grating and a Si-CCD detector (Sony ILX511b) featuring 2048 effective pixels of size $14 \times 200\ \mu m^2$, yielding a spectral resolution of 0.5 nm. The detector's exposure time was set to 1 s and 20 scans were averaged to improve the signal-to-noise ratio (SNR). The Y-axis of the spectrometer was calibrated using a standard light source (SL1 Tungsten Halogen). Quartz transmissivity was considered during the calibration process. The GE214 quartz material has over 80% transmissivity for the UV-Vis range (>90% for 300–800 nm) considered here.

Time-averaged flame images were also recorded with two intensified cameras, LaVision Imager *intense* (Sony ICX285AL sensor and Hamamatsu HB1058 intensifier), fitted with different bandpass filters chosen to target specific excited radicals. The image resolution is 6.2 pixels/mm, resulting in a field of view of 50 mm (axial, y) by 80 mm (radial, x) relative to the edge and centreline of the burner exit nozzle, respectively. Fig. 2 shows inverse Abel transformed flame images corresponding to OH* near 309 nm, NH* near 336 nm, the α band of NH_2 near 630 nm, CH* near 430 nm, and CN* near 355 nm for a stoichiometric swirl flame with $X_{NH3} = 0.60$ and Re = 20,000. The images in Fig. 2 only show half of the cross profile of the swirl flame, which is semi-axisymmetric. The intensities of the species have been normalized by the maximum. These images highlight the typical V-shape adopted by the swirl flames and confirm the contributions from multiple excited radicals to the flame's spontaneous emission of light. These images also show that different excited radicals emit from different locations in the flame, specifically NH_2*. However, as a first step, this study focuses on the spatially-integrated but spectrally-resolved chemiluminescence, which justifies the use of a spectrometer and the position of the optical fiber.

2.3. Exhaust gas analysis

Exhaust emissions (NO, N_2O, NO_2, NH_3, CO, CO_2, O_2 and H_2O) were measured using a bespoke quantum cascade laser analyzer (Emerson CT5100) operating at 463 K with a sampling frequency of 1 Hz (±1%, 0.999 linearity). Dilution of the sample by N_2 was adopted (±10% repeatability) when wet readings were above the analyzer's detection range. An isokinetic funnel with an intake diameter of 30 mm was fixed 50 mm above the quartz confinement's exit to capture homogeneous samples from the exhaust for selected operating conditions. All the emissions data reported here were recorded and averaged over a period of 120 s. Only NO emissions data are presented here, and the analysis of the other species is left to a future study.

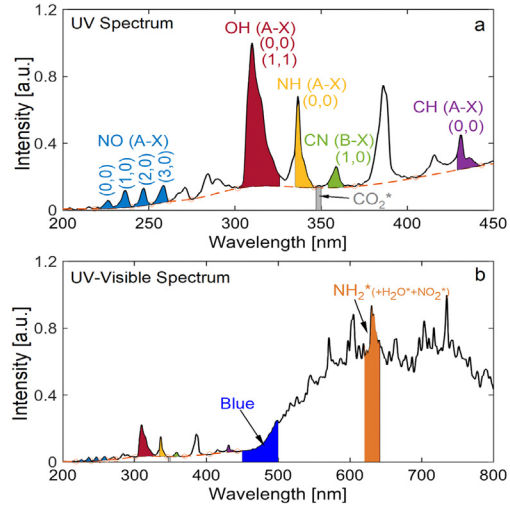

Fig. 3. (a) UV and (b) UV+visible chemiluminescence spectra for a stoichiometric swirl flame with $X_{NH3} = 0.60$ and Re = 20,000.

3. Results and discussion

3.1. Chemiluminescence spectra and intensity of single species/spectral ranges

The measured chemiluminescence spectrum of a stoichiometric swirl flame with $X_{NH3} = 0.60$ and Re = 20,000 is shown in Fig. 3. Fig. 3a and 3b shows the UV and UV+visible ranges, respectively. Expected features of the UV spectrum are found [16], namely contributions from NO*, OH*, NH*, CO_2*, CN*, and CH*. Overlay of the simulated spectra (by LIFbase) and the measured spectra (with CO_2* background removed) for this condition is provided in Supplementary Material, Fig. S3. Excellent agreement between the locations of simulated and measured peaks is found, which is deemed sufficient to properly assign species to each spectral emission. However, simulations for NH* and NH_2* are not available. Reader is referred to [13,15] for NH_2* and [16] for NH* spectra. The broadband but featureful visible spectrum typically attributed to the α band of NH_2 and H_2O is also found in Fig. 3b. Radical C_2* is also featured but its contribution is dwarfed by that of the α band of NH_2 for

the same wavelength range (~516 nm) for all flames featuring ammonia. For this reason, C_2^* will not be investigated further in this study.

In this study, contributions from different species, or specific spectral ranges, were quantified by integration of the chemiluminescence spectra over some specified wavelength ranges, highlighted with colors in Fig. 3. These ranges are 221–261 nm for NO^*, 302–326 nm for OH^*, 335–346 nm for NH^*, 347–350 nm for CO_2^*, 354–363 nm for CN^*, 429–443 nm for CH^*, 450–500 nm for *Blue* and 622–642 nm for NH_2^*. Range 450–500 nm was labeled *Blue* instead of being assigned to a specific species because multiple species, including at least CO_2^* and NH_2^*, contribute to this range. The above ranges were chosen to minimize interferences between different species. For example, the strong peak from CN^* near 380 nm was not used because CH^* also emits in this range. Because of the broadband nature of CO_2^*'s emission, it's contribution to the spectrum (see orange dashed line in Fig. 3a) was subtracted before the quantification of other excited radicals in the UV. This was also done for the laminar flames in [1].

As shown in Fig. 3b, the intensity is much larger in the visible than in the UV. Therefore, the use of a single spectrometer to simultaneously cover the 200–800 nm range led to a compromise on SNR in the UV. Indeed, the 1-s exposure time chosen to cover the full dynamic range available for this spectrometer without saturating anywhere meant that SNR could not be optimal in the UV. To give an idea of the precision of the instrument, the coefficients of variation, defined as the standard deviation divided by the mean, are 3.61% (NO^*), 3.67% (OH^*), 3.47% (NH^*), 3.60% (CN^*), 3.83% (CO_2^*), 3.40% (CH^*), 3.46% (*Blue*), 3.38% (NH_2^*) if mean values are taken for the stoichiometric swirl flame with $X_{NH3} = 0.60$ and $Re = 20{,}000$.

As discussed in [16], another important source of error is associated to the imperfect prescription of gas mass flow rates. Indeed, for all the spectral ranges defined above, the chemiluminescence intensity is sensitive to the ammonia fuel fraction and equivalence ratio (see later). To improve the readability of graphs, error bars attributed to the prescription of mass flow rates will not be plotted but their size can be computed by considering the sensitivity of chemiluminescence intensities to X_{NH3} and Φ for each condition and a 1% error on X_{NH3} and Φ. Finally, a small uncertainty may arise from the selection of the control points and of the interpolation method for the CO_2^* background calculation. However, Zhu et al. [16] showed that this source of errors is much less important than the other sources described earlier.

Fig. 4 plots the measured spectrally-integrated chemiluminescence intensities for different radicals as a function of equivalence ratio ($0.6 \leq \Phi \leq 1.3$) for different ammonia fuel fractions ($0 \leq X_{NH3} \leq 0.7$) and $Re = 20{,}000$. Color gradients are used to differentiate the changing ammonia mol fraction, i.e., the darker the color of a curve, the larger the X_{NH3}. By design, this is almost the same range of X_{NH3} and Φ than that examined for laminar flames in [16]. Except for *Blue* and NH_2^*, all excited radicals exhibit a bell-shaped curve and trends of intensity as a function of X_{NH3} and Φ are identical to that found for laminar flames in [16]. Specifically, NO^*, OH^*, and CO_2^* peak at a smaller equivalence ratio than NH^*, CN^* and CH^*. This is an important feature that suggests that well-selected ratios of chemiluminescence intensities would be very sensitive to equivalence ratio. This will be examined in the next subsection. In addition, intensities decrease monotonically as X_{NH3} increases for OH^*, CO_2^*, and CH^* (the species featured in pure methane-air flames) while the trend is non-monotonic for NO^*, NH^*, and CN^* (the species not featured in pure methane-air flames).

If $X_{NH3} \geq 0.4$, curves are bimodal for *Blue* and NH_2^*, suggesting that multiple species contribute to chemiluminescence within the corresponding spectral ranges and that these species feature different sensitivities to Φ and, perhaps, X_{NH3}. As discussed above, it is suspected that both CO_2^* and NH_2^* contribute to *Blue*. NH_2^* and H_2O are the two most likely contributors to the 622–642 nm range [13] but we will continue to refer to it as only NH_2^* for simplicity and for consistency with previous studies (e.g., [15]).

3.2. Chemiluminescence intensity ratios

Chemiluminescence intensity ratios from two different excited radicals (or spectra ranges) cancel out effects of varying flame surface area, which is a characteristic inherent in turbulent flames. Therefore, if practical flames are the target, it is useful to examine chemiluminescence intensity ratios as well. We defined 8 excited radicals (or spectral ranges) in the range 200–800 nm, yielding 28 possible different ratios. These were all examined but only 7 were found to be of practical relevance. They are plotted in Fig. 5 as a function of Φ for different X_{NH3} and in Fig. 6 as a function of the Re for different Φ and X_{NH3}. The coefficients of variation calculated for the 7 intensity ratios are as follows: 0.48% (OH^*/CH^*), 0.40% (CH^*/OH^*), 0.35% (CN^*/NO^*), 0.40% (NH^*/CH^*), 0.39% (NH^*/OH^*), 0.41% (CH^*/NH^*), 0.57% (Blue/NH_2^*) if mean values are taken for the stoichiometric swirl flame with $X_{NH3} = 0.60$ and $Re = 20{,}000$.

OH^*/CH^*: The OH^*/CH^* intensity ratio is routinely used to sense Φ in pure methane-air flames (e.g. [23]). This capability is confirmed by Fig. 5a because this ratio decreases rapidly when Φ increases if $X_{HN3} = 0$. The sensitivity of this ratio decreases when X_{HN3} increases, which limits its sensing capability in flames featuring ammonia. In addition, curves in Fig. 5a do not overlap, meaning

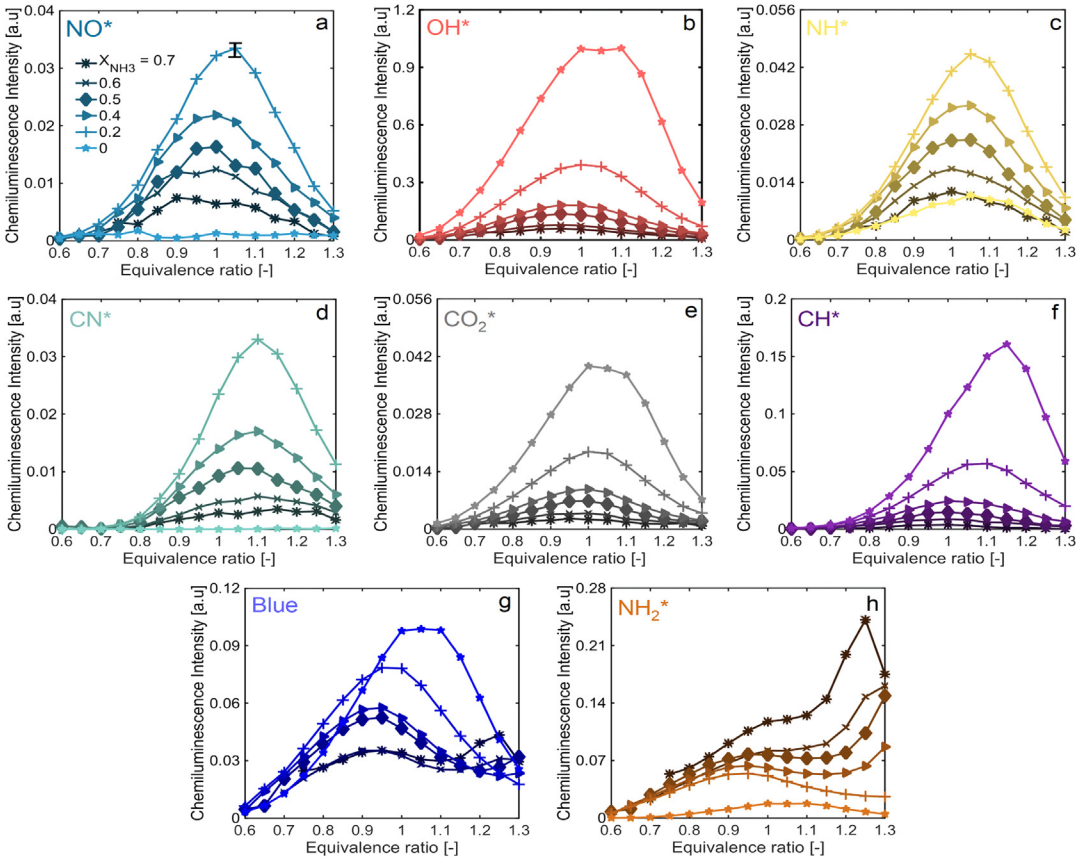

Fig. 4. Measured chemiluminescence intensity of 8 excited radicals (or spectral ranges) as a function of equivalence ratio for different ammonia fuel fractions and Re = 20,000.

that this ratio cannot be used if the fuel composition is not known. Fig. 6a shows that this ratio is not modified significantly by the Reynolds number, especially considering that the latter was multiplied by 4. This is true for different equivalence ratios (Φ = 0.8, 1.0, and 1.2) and ammonia fractions (X_{NH3} = 0.30 and 0.45).

CN*/OH*: This ratio is available as long as there is some ammonia in the fuel blend and it increases monotonically and rapidly when Φ increases. To illustrate, it increases by ~1055% when Φ increases from 0.7 to 1.2. It is also fairly insensitive to X_{NH3} for the range considered here. This is why this ratio was proposed as a surrogate for equivalence ratio in [16], albeit for laminar flames. The tighter collapses of all curves on a single one in [16] suggests that discrepancies observed here for turbulent flames can be attributed to the lower precision of the instruments. Regardless, discrepancies associated to the imperfect overlap of curves featuring different X_{NH3} only translates into a ±6% uncertainty on Φ at Φ = 1. The same way that it was found insensitive to strain rate in counterflow laminar flames, Fig. 6b shows that ratio CN*/OH* is unaffected by Re, at least over the range examined here. For the above reasons, CN*/OH* is a very promising ratio for sensing equivalence ratio in practical flames, even if the Re and X_{NH3} are unknown/varying, as long as $X_{NH3} \geq 0.20$.

CN*/NO*: Ratio CN*/NO* was described in [16] as a suitable equivalence ratio surrogate if $0.05 \leq X_{NH3} \leq 0.50$. Data recorded here for turbulent flames are consistent with this description given that this ratio also increases monotonically and rapidly when Φ increases (see Fig. 5c) and is insensitive to X_{NH3} (if $0.20 \leq X_{NH3} \leq 0.5$) and Re (see Fig. 6c). Discrepancies associated with the imperfect overlap of curves featuring different X_{NH3} translates into a ±5% uncertainty on Φ at Φ = 1 if only curves with $0.20 \leq X_{NH3} \leq 0.50$ are considered.

NH*/CH*: Fig. 5d shows that ratio NH*/CH* has the potential to sense X_{NH3} in ammonia-methane-air swirling flames because it exhibits a large sensitivity to X_{NH3} and is only moderately sensitive to Φ, except for the smallest (X_{NH3} = 0) and largest ammonia fractions ($X_{NH3} \geq 0.60$) considered. For these "extreme" ammonia fractions,

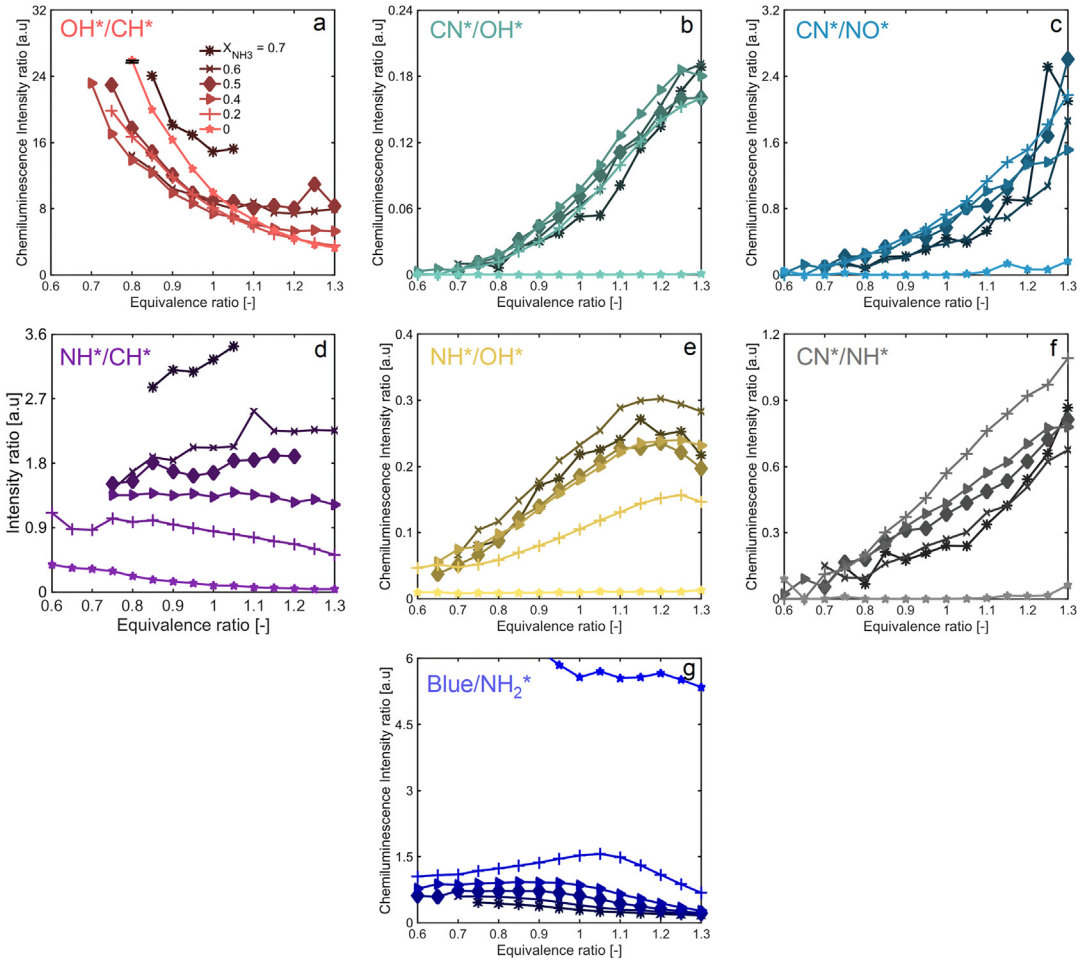

Fig. 5. Seven measured ratios of chemiluminescence intensities as a function of equivalence ratio for different ammonia fuel fractions and Re = 20,000.

knowledge of the equivalence ratio, e.g., obtained via measurement of ratio CN*/OH*, would be necessary to infer X_{NH3} accurately. The exact same trends were observed for laminar flames in [16]. Like the previous ratios examined, ratio NH*/CH* is marginally sensitive to Re (see Fig. 6d), which support its use for sensing turbulent flames. The large sensitivity of ratio NH*/CH* to X_{NH3} can be explained by the fact that NH* and CH* are not featured in pure methane-air and ammonia-air flames, respectively.

NH*/OH* & CN*/NH*: In [16], Zhu et al. also proposed to combine the use of ratios NH*/OH* and CN*/NH* to infer Φ and X_{NH3} simultaneously in laminar ammonia-methane-air flames. This was possible because both ratios monotonically increased when Φ increased but featured an opposed sensitivity to X_{NH3} (as long as $X_{NH3} > 0$). Even though the smallest precision of the instrument used here makes the argument less compelling, it is also valid for turbulent flames (see Fig. 5e and f). Using these ratios to sense Φ and X_{NH3} simultaneously with an acceptable accuracy requires a better precision than that exhibited here, which could easily be achieved by optimizing the spectrometer's settings to the UV range only, like in [16]. While ratio CN*/NH* is insensitive to Re over the large range examined here (see Fig. 6e), ratio NH*/OH* increases more substantially when Re is increased (see Fig. 6f), which could be a source of uncertainty in flames featuring unknown or large variations of Re.

***Blue*/NH_2*:** Contrary to in [16], the visible range was examined here and ratio *Blue*/NH_2* is available. It is very sensitive to X_{NH3}, especially for the most modest ammonia fractions, and much less sensitive to Φ (see Fig. 5g). This suggests that ratio *Blue*/NH_2* could be a great surrogate for X_{NH3}, as long as Φ is measured with another ratio, even with a modest accuracy. Unfortunately, this ratio is

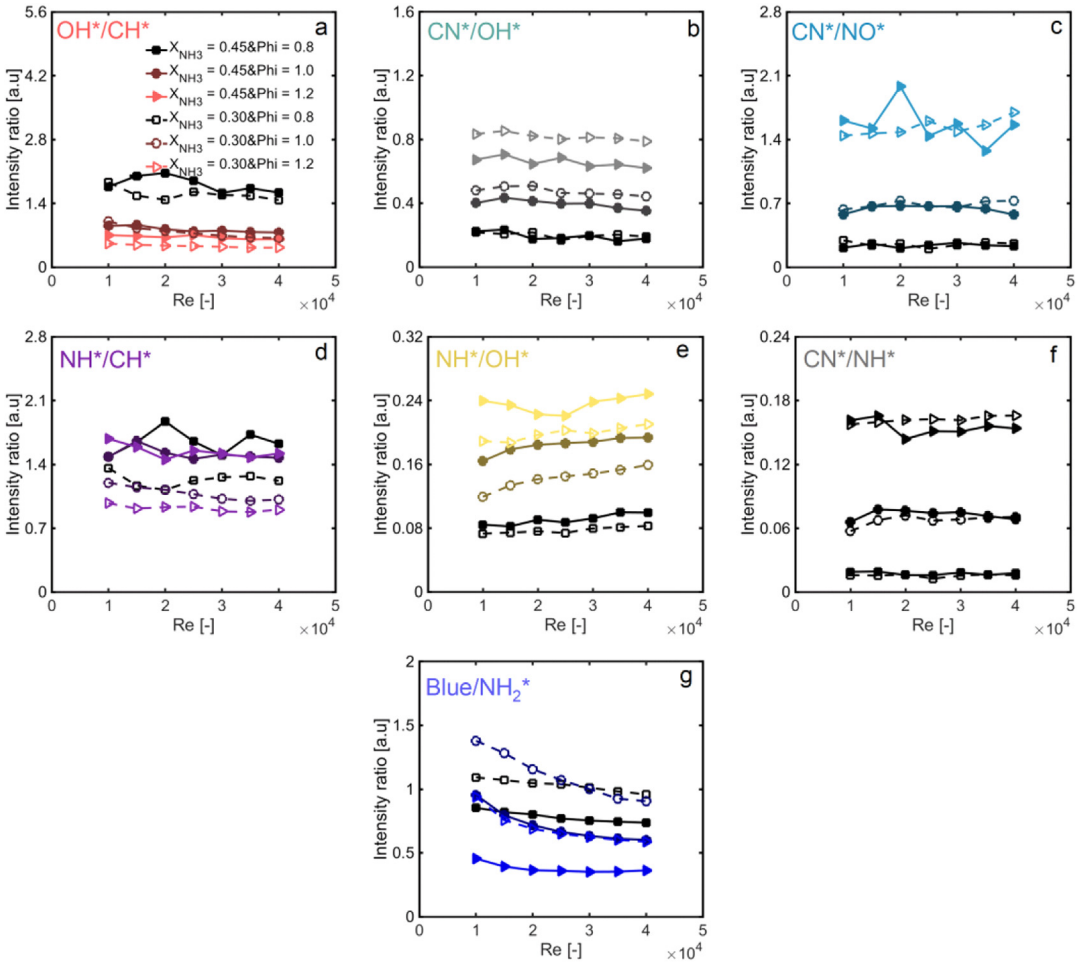

Fig. 6. Seven measured ratios of chemiluminescence intensities as a function of Reynolds number for different ammonia fuel fractions and equivalence ratios.

quite sensitive to Re (see Fig. 6g), implying that it could only be used to sense flames exhibiting small variations of Re.

3.3. *NO*/NH*/CN* chemiluminescence as a surrogate of exhaust NO emissions*

Given that exhaust NO emissions were measured, it is interesting to investigate if these could have been predicted using chemiluminescence. Fig. 7 shows the measured wet NO emissions as a function of Φ for different X_{NH3} and Re = 20,000. Trends and numbers are consistent with existing literature [24] but, more interesting, trends closely match that of NO*, NH*, and CN*. Wet NO, NO*, NH*, and CN* all peak near stoichiometric, although CN* peaks at a richer equivalence ratio, and first increase then decrease when X_{NH3} increases. This suggests that NO*, NH*, or

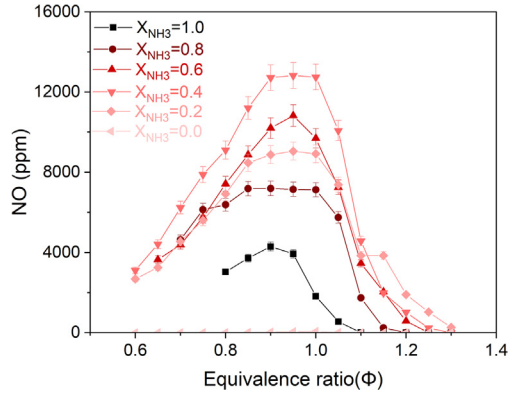

Fig. 7. Measured wet NO emissions in the exhaust as a function of equivalence ratio for different ammonia fractions and Re = 20,000.

perhaps CN* could be considered to monitor the NO emission performance of practical ammonia-methane-air flames. This is consistent with [25], where a temporal correlation was found between NO_X and NH* and CN* in an incinerator. Correlation between NO and NH* can be explained by the fact that NH* is most-likely produced, at least partly, via reaction $CH + NO \rightarrow NH^* + CO$ [26]. Similarly, CN* is most-likely produced, at least partly, via reaction $C_2 + NO \rightarrow CN^* + CO$ [27]. Provided that thermal excitation of NO is possible for the flame temperatures considered here-this should be verified-a correlation between NO and NO* is also not surprising.

Further work is needed to fully understand if chemiluminescence from NO*/NH*/CN* could be used to quantitatively monitor NO emission in practical ammonia-methane-air flames. This cannot be achieved here due to space limitations and it is left to a future study.

4. Conclusions

This study investigated the chemiluminescence footprint of swirling ammonia-methane-air flames over wide ranges of equivalence ratios, ammonia fractions in the fuel blend, and Reynolds numbers using an industrial scale burner. Important excited radicals contributing to chemiluminescence in the UV and visible ranges were confirmed, namely NO*, OH*, NH*, CN*, CO_2*, CH*, and NH_2*.

Trends of chemiluminescence intensities measured in the UV for these turbulent flames are identical to that measured previously for laminar flames of the same fuel blends. Important features include: (1) intensities from some excited radicals (OH*, CO_2*, and CH*) decrease when the ammonia fraction decreases while that from others (NO*, NH*, and CN*) first increase then decrease; (2) intensities from these radicals follow a bell-shape curve with equivalence ratio but peak for different equivalence ratios.

Trends of visible chemiluminescence are more complicated, i.e., curves as a function of equivalence ratio are bimodal if there is enough ammonia in the fuel blend, because multiple species are active for the same wavelengths. It is likely that CO_2* and NH_2* are the main contributors between 450 and 500 nm while NH_2* and H_2O are responsible for most of the orange emission, e.g., between 622 and 642 nm.

Ratios of chemiluminescence intensities were also studied because these allow removing effects of flame surface area. Also consistent with findings in laminar flames, ratios CN*/OH*, CN*/NO*, and NH*/CH* were found to be promising candidate for sensing practical ammonia-methane-air flames. Ratios CN*/OH*, CN*/NO* are potential surrogates for equivalence ratio if $X_{NH3} \geq 0.20$ and $0.05 \leq X_{NH3} \leq 0.50$, respectively. Ratio NH*/CH* is a potential surrogate for the ammonia fraction provided that equivalence ratio is roughly known. Ratio *Blue*/NH_2* is another seducing surrogate for the ammonia fraction but, contrary to CN*/OH*, CN*/NO*, and NH*/CH*, its sensitivity to Reynolds number may limits its range of applications.

Trends of exhaust NO concentration with equivalence ratio and ammonia fraction match that of NO*, NH*, and CN*, suggesting that these excited radicals could be used for the early detection of NO in practical ammonia-methane-air flames. However, more work is required to assess the accuracy and precision of such method.

Declaration of Competing Interest

The authors declare that they have no known competing financial interests or personal relationships that could have appeared to influence the work reported in this paper.

Acknowledgments

This project has received funding from the European Union 's Horizon 2020 research and innovation programme under grant agreement No 884157. The research was undertaken at the Cardiff University's Thermofluids lab (W/0.17) with invaluable technical support from Mr. Malcolm Seaborne. This study was also supported by funding from King Abdullah University of Science and Technology (KAUST) under grant number BAS/1/1370-01-01. Information on the data underpinning the results presented here, including how to access them, can be found in the Cardiff University data catalogue at http://doi.org/10.17035/d.2022.0220491548.

Supplementary materials

Supplementary material associated with this article can be found, in the online version, at doi:10.1016/j.proci.2022.08.073.

References

[1] S. Candel, Combustion dynamics and control: progress and challenges, Proc. Combust. Inst. 29 (2002) 1–28.
[2] N. Docquier, F. Lacas, S. Candel, Operating point control of gas turbine combustor, in: Proceedings of the 39th Aerospace Sciences Meeting and Exhibit, Reno, NV, USA, 2001.
[3] J.P. Hathout, M. Fleifil, A.M. Annaswamy, A.F. Ghoneim, Heat-release actuation for control of mixture-inhomogeneity-driven combustion instability, Proc. Combust. Inst. 28 (2000) 721–730.

[4] J. Ballester, T. García-Armingol, Diagnostic techniques for the monitoring and control of practical flames, Prog. Energy Combust. Sci. 36 (2010) 375–411.
[5] N. Docquier, S. Candel, Combustion control and sensors: a review, Prog. Energy Combust. Sci. 28 (2002) 107–150.
[6] A. Gaydon, H. Wolfhard, S. Penner, Flames, their structure, radiation and temperature, J. Appl. Mech. 27 (1960) 600.
[7] T. Muruganandam, et al., Optical equivalence ratio sensors for gas turbine combustors, Proc. Combust. Inst. 30 (2005) 1601–1609.
[8] B. Stojkovic, T. Fansler, M. Drake, V. Sick, High-speed imaging of OH* and soot temperature and concentration in a stratified-charge direct-injection gasoline engine, Proc. Combust. Inst. 30 (2005) 2657–2665.
[9] J.G. Lee, K. Kim, D.A. Santavicca, Measurement of equivalence ratio fluctuation and its effect on heat release during unstable combustion, Proc. Combust. Inst. 28 (2000) 415–421.
[10] A. Valera-Medina, H. Xiao, M. Owen-Jones, W.I.F. David, P.J. Bowen, Ammonia for power, Prog. Energy Combust. Sci. 69 (2018) 63–102.
[11] H. Kobayashi, A. Hayakawa, K.D.K.A. Somarathne, E.C. Okafor, Science and technology of ammonia combustion, Proc. Combust. Inst. 37 (2019) 109–133.
[12] A. Gaydon, in: The Spectroscopy of Flames, Springer, Dordrecht, Netherlands, 2012, p. 296.
[13] A. Hayakawa, T. Goto, R. Mimoto, T. Kudo, H. Kobayashi, NO formation/reduction mechanisms of ammonia/air premixed flames at various equivalence ratios and pressures, Mech. Eng. J. 2 (2015) 14–23.
[14] X. Zhu, A.A. Khateeb, T.F. Guiberti, W.L. Roberts, NO and OH* emission characteristics of very-lean to stoichiometric ammonia-hydrogen-air swirl flames, Proc. Combust. Inst. 38 (2021) 5155–5162.
[15] D. Pugh, et al., An investigation of ammonia primary flame combustor concepts for emissions reduction with OH*, NH2* and NH* chemiluminescence at elevated conditions, Proc. Combust. Inst. 38 (2021) 6451–6459.
[16] X. Zhu, A.A. Khateeb, W.L. Roberts, T.F. Guiberti, Chemiluminescence signature of premixed ammonia-methane-air flames, Combust. Flame 231 (2021) 111508–111522.
[17] Y. Yoshida, H. Kakinuma, Y. Kotani, Extinction of turbulent premixed flames by small-scale turbulence at Kolmogorov microscale, Proc. Combust. Inst. 26 (1996) 397–404.
[18] C.K. Law, Dynamics of stretched flames, Proc. Combust. Inst. 22 (1989) 1381–1402.
[19] N. Peters, Laminar flamelet concepts in turbulent combustion, Proc. Combust. Inst. 21 (1988) 1231–1250.
[20] S. Ishizuka, On the behavior of premixed flames in a rotating flow field: establishment of tubular flames, Proc. Combust. Inst. 20 (1985) 287–294.
[21] X. Zhu, X. Xia, P. Zhang, Near-field flow stability of buoyant methane/air inverse diffusion flames, Combust. Flame 191 (2018) 66–75.
[22] X. Jiang, K.H. Luo, Dynamics and structure of transitional buoyant jet diffusion flames with side-wall effects, Combust. Flame 133 (2003) 29–45.
[23] C.S. Panoutsos, Y. Hardalupas, A.M.K.P. Taylor, Numerical evaluation of equivalence ratio measurement using OH∗ and CH∗ chemiluminescence in premixed and non-premixed methane–air flames, Combust. Flame 156 (2009) 273–291.
[24] E.C. Okafor, et al., Control of NOx and other emissions in micro gas turbine combustors fuelled with mixtures of methane and ammonia, Combust. Flame 211 (2020) 406–416.
[25] A. Leipertz, R. Obertacke, F. Wintrich, Industrial combustion control using UV emission tomography, Proc. Combust. Inst. 26 (1996) 2869–2875.
[26] A. Bergeat, T. Calvo, N. Daugey, J.C. Loison, G. Dorthe, Product branching ratios of the CH + NO reaction, J. Phys. Chem. A 102 (1998) 8124–8130.
[27] A. Fontijn, Mechanism of CN and NH chemiluminescence in the N-O-C_2H_2 and O-NO-C_2H_2 reactions, J. Chem. Phys. 43 (1965) 1829–1830.